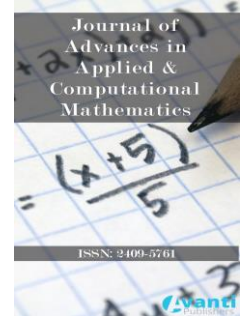









Published by Avanti Publishers  
**Journal of Advances in Applied &  
Computational Mathematics**

ISSN (online): 2409-5761



---

## Landslide Hazard Assessment Model for Slope Stability Analysis

Giulia De Santis <sup>1</sup>, Nadaniela Egidì <sup>2</sup>, Josephin Giacomini <sup>2,\*</sup>, Eleonora Gioia <sup>3</sup>,  
Pierluigi Maponi <sup>2</sup> and Lorenza Spadoni<sup>2</sup>

<sup>1</sup>Department of Industrial Engineering and Mathematical Sciences, Polytechnic University of Marche, via Breccia Bianche 12, 60131 Ancona (AN), Italy


<sup>2</sup>School of Science and Technology - Mathematics Division, University of Camerino, Via Madonna delle Carceri 9, 62032 Camerino (MC), Italy

<sup>3</sup>Department of Methods and Models for Economics, Territory, and Finance, Sapienza University of Rome, Via del C. Laurentiano 9, 00161, Rome, Italy

---

### ARTICLE INFO

Article Type: Research Article

Academic Editor: Ahmed Saad Rashed 

Keywords:

Sliding

Slope stability

Factor of safety

Limit equilibrium analysis

Timeline:

Received: July 19, 2023

Accepted: October 06, 2023

Published: November 01, 2023

Citation: De Santis G, Egidì N, Giacomini J, Gioia E, Maponi P, Spadoni L. Landslide hazard assessment model for slope stability analysis. J Adv App Comput Math. 2023; 10: 77-87.

DOI: <https://doi.org/10.15377/2409-5761.2023.10.8>

### ABSTRACT

Soil moisture dynamics is a complex phenomenon that depends on the atmospheric conditions, the geomorphological characteristics of the region under study, and the corresponding land use. It can be formally described by a diffusion model based on Darcy's law and the law of mass continuity. In this work, the obtained numerical solution of the hydrological model has been exploited to evaluate the soil moisture in a given region and build a risk map for the slope stability of this region. More in detail, the infinite slope model from slope stability analysis has been used for evaluating the safety factor and constructing the corresponding quantitative hazard maps. Some results of the proposed method applied to a real case study are shown and discussed.

---

\*Corresponding Author

Email: [josephin.giacomini@unicam.it](mailto:josephin.giacomini@unicam.it)

# 1. Introduction

Slope instability is widely recognized as an ever-present danger [1, 2]: in fact, landslides are frequent disasters and constitute an important and costly problem. Europe itself, due to its geography, has many highly hazardous regions [3], since landslides are a major hazard in most mountainous and hilly regions. Furthermore, intense and/or long-lasting rainfalls represent the most frequent triggers of landslides [4, 5]. Nowadays, a large body of knowledge, which concerns various parameters, variables, and models that are important to a clear understanding of the processes affecting the stability/instability of natural slopes, is available [6-9]. Nevertheless, actual methods for landslide evaluation are mainly based on scientific literature of geomorphologic studies and historical landslide events.

In this work, the relation between the stability and the hydrological conditions of a considered region is investigated. The slope failure hazard during rainfall events is analyzed by simultaneously considering a hydrological model for evaluating the soil water content and a stability model for landslide forecasting. In the formalization of hydrodynamic problems, the most famous model involves the Navier-Stokes equations and, eventually, the heat equation [10, 11]. On the other hand, hydrological problems must take into consideration the porous medium, which strongly modifies the behavior of the flow. In this case, a proper model is based on Richard's equation [12-14]. In the hydrological model considered in this paper, the following classical assumptions are made:

- the infiltration capacity of the soil always exceeds the rainfall intensity, so the groundwater table rises when the rainfall infiltrates; this means that the water does not run off and the soil can catch all the water from rainfall, even when heavy rainfall occurs, and the water table rises unless the soil is saturated; in addition, run-off yields erosion and flooding but does not affect the landslide hazard;
- flow from or inside bedrock is not considered [15].

In the literature, there are various methods for slope stability analysis, such as *the method of slices* and *the limit equilibrium analysis model*, [16] for an overview of these models. In this preliminary work, the *infinite slope model* has been used as a stability model, which is a simple method inside the general limit equilibrium analysis model. However, another interesting method, which can be used when the three-dimensional case is considered, is the one shown in [17], where the force and moment limit equilibrium analysis is used to produce a three-dimensional slope stability analysis. In this method, a potential sliding mass is divided into a group of square soil columns, which will be henceforth called sections, and the equilibrium analysis model allows:

- to work in areas of irregular geometrical and/or geological conditions, where the direction of potential sliding may vary considerably and be difficult to guess in advance;
- to avoid establishing local coordinate systems for various potential failure surfaces.

This study was part of the European project "LANDSLIDE: Landslide risk assessment model for disaster prevention and mitigation". The objectives of the LANDSLIDE project are:

- the development of a Landslide Hazard Assessment Model and Software for shallow landslide events triggered by rainfalls, that predicts, based on weather forecasts, the corresponding landslide hazard and sends this prediction to appropriate territorial authorities;
- the test and the transfer of the Landslide Hazard Assessment Model and Software into the civil protection systems of the partner territories evolved;
- the involvement of other sectors concerned in risk prevention and mitigation, enabling them to consider risk prevention in their respective planning and development policies;
- the involvement of people directly affected by the identified risks, to make them engaged in self-protection and prevention activities.

The following of the paper is structured as follows. Section 2 defines the factor of safety  $F$  and the infinite slope model for its computation. Section 3 illustrates the hydrological model used for computing the soil moisture. Section 4 reports the discretization scheme. Section 5 contains the numerical results obtained from a case study. Section 6 gives final remarks and shows possible developments of this work.

## 2. The Factor of Safety $F$ and the Stability Model

The *infinite slope model* is used in this paper as a mathematical model for slope stability analysis used in this work. The infinite slope model allows, starting from the soil characteristics and the water content, the computation of the *factor of safety*  $F$ . Such  $F$  is the ratio between forces that prevent the slope from sliding down and those that bring the slope to collapse and measures the resistance of inclined surfaces to failure by sliding or collapsing. Roughly speaking, a factor of safety larger than 1 indicates stable conditions, whereas a factor of safety smaller than 1 indicates unstable ones. When  $F = 1$ , the slope is at the point of failure. Therefore, the factor of safety  $F$  is a hazard index and its numerical evaluation is required to obtain quantitative hazard maps.

### 2.1. The Factor of Safety $F$

The following expression of the factor of safety  $F$  at a section of the soil can be obtained from the Mohr-Coulomb's law [18, 19]:

$$F = \frac{c' + (\sigma_n - u_n) \tan(\phi)}{s}, \quad (1)$$

where  $c'$  is the cohesion,  $\sigma$  is related to the total force applied on the section base  $\sigma_n$  is its normal component,  $u$  is related to the uplifting force at the failure surface that consists in the pore-fluid pressure and  $u_n$  is its normal component,  $\phi$  is the angle of shearing resistance or friction angle, and  $s$  is related to the driving force and is called ultimate shear stress. Hence,  $F$  is the ratio between the resisting force and the driving force. More in detail, the resisting force is composed of two addenda: the cohesion  $c'$ , which includes some attractions among the particles (perhaps at the molecular level) that give shearing resistance even at zero effective stress, see [20] for more details; the friction  $(\sigma_n - u_n) \tan(\phi)$ , which is the shear strength of soil along the failure surface. In particular, the frictional resistance to movement depends on  $\sigma$  and  $u$ , in fact, the friction is related to the soil grain contact forces and it is reduced by the pressure  $u$  of a fluid in the soil pores, since it reduces the grain-to-grain contact loads.

### 2.2. The Infinite Slope Model

Suppose that each soil section is a large slope having uniform steepness and geological features. Under these assumptions, the *infinite slope model* [21] can be leveraged to describe the stability of the considered section by using an "infinitely large failure plane", approximately parallel to the slope surface. Hence,  $F$  can be computed in a bi-dimensional grid (one point for each vertical section) on the slope surface, each discretization point is considered a homogeneous unit, and the effect of the neighboring discretization points (sections) is not considered.

The infinite slope model is based on the so-called limit equilibrium analysis, where a granular material (like soil) is subjected to forces that cannot move the material but can deform it. In the case of soil, the usually involved forces are gravity and seismic waves, and the corresponding deformations may produce landslides. In particular, with the infinite slope model, it can be evaluated when this deformation starts, but there is no information about the dynamics of this deformation under the action of the forces.

Let us note that, from Formula (1), the resisting stress due to friction  $(\sigma_n - u_n) \tan(\phi)$  depends on the component of the effective stress  $\sigma - u$  normal to the failure surface, where  $\sigma$  is the total stress.

In the infinite slope model, the following assumptions hold:

- the *total stress*  $\sigma$  is equal to the sum of the weights of the soil section and of the water contained in it;
- the *driving force*  $s$  is equal to the component of the total stress  $\sigma$  tangent to the failure surface.

The resulting formula for the safety factor, see [22] for details, is then

$$F = \frac{C + (z\gamma - z_w\gamma_w) \cos^2(\beta) \tan(\phi)}{z\gamma \sin(\beta) \cos(\beta)}, \quad (2)$$

where

- $C$  is the effective cohesion;
- $\gamma_w$  is the unit weight of water, in  $[kN/m^3]$ , and it is equal to 9.81;
- $\gamma$  is the unit weight of the soil, in  $[kN/m^3]$ ;
- $z$  is the depth of the failure surface, in  $[m]$ ;
- $z_w$  is the height of the groundwater table above the failure surface, in  $[m]$ ;
- $\beta$  is the slope of the inclined surface;
- $\phi$  is the angle of internal friction.

The water content, obtained from the hydrological model, is used for computing  $F$  by (2) and obtaining information about the stability of the slope surface at each point, and this results in a *landslide hazard map*.

### 3. The Hydrological Model

The water infiltration into the soil can be formally described by Richard's equation [12] and arises from Darcy's law [23] and the mass conservation equation. Richard's equation is a partial differential equation defining the water flow in saturated or unsaturated porous media. In particular, if  $(x, y, z) \in \Omega \subseteq \mathbb{R}^3$  and  $t$  is the time variable, then Richard's equation has the following form

$$\left( C(h-z) + S \frac{\theta(h-z)}{n_\epsilon} \right) \frac{\partial h}{\partial t} = \frac{\partial}{\partial x} \left( K(h-z) \frac{\partial h}{\partial x} \right) + \frac{\partial}{\partial y} \left( K(h-z) \frac{\partial h}{\partial y} \right) + \frac{\partial}{\partial z} \left( K(h-z) \frac{\partial h}{\partial z} \right) + W - ET, \quad (3)$$

where:

- $n_\epsilon$  is the porosity;
- $h = h(x, y, z, t)$  is the hydraulic head at point  $(x, y, z) \in \Omega$  at time  $t$ ;
- $\psi = h - z$  is the pressure head;
- $\theta(\psi)$  is the water content, which is equal to the ratio between the volume of water and the total volume

$$\theta = \frac{V_w}{V};$$

the water content  $\theta$  is related to the saturation of the porous medium and since, in real physical situations, it is very difficult to achieve complete saturation as well as a moisture-free soil,  $\theta_s$  denotes the saturated water content, and  $\theta_r$  the residual water content in the soil;

- $C(\psi) = \frac{d\theta}{d\psi}$  is the specific capillary capacity;
- $K(\psi)$  is the hydraulic conductivity;
- $S$  is the storage coefficient;
- $W$  is the recharge and is related to the rate of precipitation [23, 24];
- $ET$  is the evapotranspiration and represents the loss of water due to evaporation and transpiration of plants; it can be estimated by the *Penman-Montieth equation* [24, 25].

Although both  $\theta$  and  $K$  are complicated nonlinear functions, there are a few fairly standard forms that are used to define them. Popular forms for them are due to Van Genuchten [26-28] and are given by the following formulas:

$$\frac{\theta(\psi) - \theta_r}{\theta_s - \theta_r} = \begin{cases} \left(\frac{1}{1 + |\alpha\psi|^n}\right)^m, & \text{if } \psi < 0, \\ 1, & \text{if } \psi \geq 0, \end{cases} \quad (4)$$

$$K(\psi) = \begin{cases} K_s [1 - (\alpha\psi)^n]^{-\frac{m}{2}} \left[1 - \left(\frac{|\alpha\psi|^n}{1 + |\alpha\psi|^n}\right)^m\right]^2, & \text{if } \psi < 0, \\ K_s, & \text{if } \psi \geq 0, \end{cases} \quad (5)$$

where

- $\alpha$  is the inverse of the pressure head  $\psi_0$  at the air-entry point;
- parameters  $n$  and  $m$  are empirical quantities such that  $n \cdot m = n - 1$ ;
- $K_s$  is the value of the permeability when the soil is saturated.

Note that, from Formula (4), it is possible to distinguish between saturated and unsaturated soil according to the value of the pressure head  $\psi$ : if  $\psi < 0$ , the soil is unsaturated; if  $\psi \geq 0$  the soil is saturated. In addition, since all the above-described hydraulic parameters are related to the pore size distribution and pore geometry, they depend on the medium, i.e., on the type of considered soil.

Equation (3) can be numerically solved by considering appropriate initial and boundary conditions. In the next section, a suitable discretization is given when  $\Omega$  is the basin taken into account and  $[0, L_t]$  is the time interval of observation, see [29] for more details. Finite difference schemes for Richard's equation can be found in [30-32], whereas finite element schemes on fixed spatial grids are adopted in [33-35] and an adaptive approach is shown in [36]. Another discretization scheme for Richard's equation that can be adaptable in parallel computing can be seen in [37].

## 4. The Discretization Method for the Hydrological Model

To numerically solve Equation (3), the central finite difference scheme for the space derivatives approximation is applied. To accomplish this goal, the considered region  $\Omega$  should satisfy

$$\Omega \subseteq [0, L_x] \times [0, L_y] \times [0, L_z] \subseteq \mathbb{R}^3. \quad (6)$$

Let  $N_x, N_y, N_z$  be positive integers. Then, the following discretization steps can be defined along the  $x$ ,  $y$ , and  $z$  directions,  $\Delta x = L_x/N_x$ ,  $\Delta y = L_y/N_y$  and  $\Delta z = L_z/N_z$ , respectively. These discretization steps define the partitions of the intervals  $[0, L_x]$ ,  $[0, L_y]$  and  $[0, L_z]$ , respectively, and the corresponding nodes are

$$\begin{aligned} x_i &= i\Delta x, & \forall i &= 0, 1, \dots, N_x, \\ y_j &= j\Delta y, & \forall j &= 0, 1, \dots, N_y, \\ z_k &= k\Delta z, & \forall k &= 0, 1, \dots, N_z. \end{aligned} \quad (7)$$

Fig. (1) shows the 3D space approximation around the point corresponding to the indices  $(i, j, k)$  as well as its stencil, used in the finite difference scheme. To obtain the approximated solution, the time domain, supposed to be  $[0, L_t]$ , needs to be discretized, too. The time interval is partitioned by the nodes

$$t_n = n\Delta t, \quad \forall n = 0, 1, \dots, N_t, \quad (8)$$

where  $N_t$  is a positive integer and  $\Delta t = L_t/N_t$  is the corresponding time step. From now on, the following notation is adopted: given a function  $g(x, y, z, t)$ , for  $i = 0, 1, \dots, N_x$ ,  $j = 0, 1, \dots, N_y$ ,  $k = 0, 1, \dots, N_z$ , and  $n = 0, 1, \dots, N_t$ ,

$$g_{i,j,k}^n = g(x_i, y_j, z_k, t_n).$$

Similarly, when  $g$  does not depend on  $t$ ,

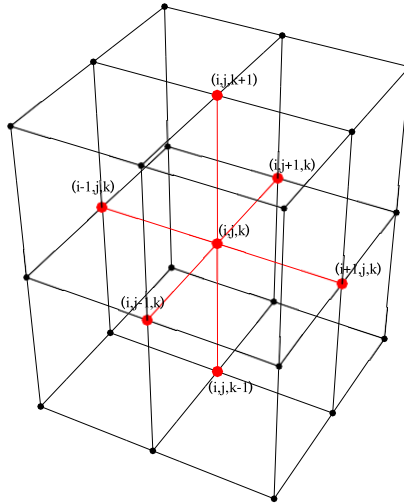


**Figure 1:** Space approximation and stencil (in red) of the point corresponding to the indices  $(i, j, k)$  in the finite difference scheme.

$$g_{i,j,k} = g(x_i, y_j, z_k).$$

So, leveraging the central differences for the first order space derivatives, with half discretization step, from Equation (3) it follows

$$\begin{aligned} & \left( C_{i,j,k}^n + S \frac{\theta_{i,j,k}^n}{n_\epsilon} \right) \frac{\partial h}{\partial t}(x_i, y_j, z_k, t_n) \\ & \approx \frac{1}{(\Delta x)^2} \left[ K_{i+\frac{1}{2},j,k}^n (h_{i+1,j,k}^n - h_{i,j,k}^n) - K_{i-\frac{1}{2},j,k}^n (h_{i,j,k}^n - h_{i-1,j,k}^n) \right] \\ & + \frac{1}{(\Delta y)^2} \left[ K_{i,j+\frac{1}{2},k}^n (h_{i,j+1,k}^n - h_{i,j,k}^n) - K_{i,j-\frac{1}{2},k}^n (h_{i,j,k}^n - h_{i,j-1,k}^n) \right] \\ & + \frac{1}{(\Delta z)^2} \left[ K_{i,j,k+\frac{1}{2}}^n (h_{i,j,k+1}^n - h_{i,j,k}^n) - K_{i,j,k-\frac{1}{2}}^n (h_{i,j,k}^n - h_{i,j,k-1}^n) \right] + W_{i,j,k}^n - ET_{i,j,k}^n, \end{aligned} \tag{9}$$

for  $i = 0, 1, \dots, N_x, j = 0, 1, \dots, N_y, k = 0, 1, \dots, N_z$ , and  $(x_i, y_j, z_k) \in \Omega, n = 0, 1, \dots, N_t - 1$ , where values of discretized function  $K$  at non-integer indices are obtained by the average of the same function at integer indices.

To be solved, Equation (9) must be completed with boundary conditions. In particular, the zero normal flow condition is imposed at the boundary  $\partial\Omega$ , that is the Neumann condition:

$$\frac{\partial h}{\partial \hat{n}}(x, y, z, t) = 0,$$

where  $(x, y, z)$  is a point on  $\partial\Omega$  and  $\hat{n}$  is the outward unit normal vector. For example: if  $(x_i, y_j, z_k)$  is one of these boundary points and  $(x_{i-1}, y_j, z_k) \notin \Omega$ , then the discretized Neumann boundary condition with normal direction parallel to the  $x$  coordinate axis gives

$$h_{i-1,j,k}^n \approx h_{i,j,k}^n.$$

With an abuse of notation, the same symbol  $h_{i,j,k}^n$  denotes the unknown and its approximation. Hence Equation (9) and boundary conditions can be also expressed as follows

$$\frac{\partial \underline{h}^n}{\partial t} = \underline{F}(\underline{h}^n, t_n), \tag{10}$$

where:

- for  $n = 0, 1, \dots, N_t$ ,  $\underline{h}^n$  is the vector whose entries are  $h_{i,j,k}^n$ ,  $i = 0, 1, \dots, N_x$ ,  $j = 0, 1, \dots, N_y$ ,  $k = 0, 1, \dots, N_z$ , such that  $(x_i, y_j, z_k) \in \Omega$ ,
- $\underline{F}(\underline{h}, t)$  is the nonlinear vectorial function obtained from (9) and the boundary conditions.

By applying the Crank-Nicolson Method to (10) it follows

$$\underline{h}^{n+1} = \underline{h}^n + \frac{\Delta t}{2} (\underline{F}(\underline{h}^n, t_n) + \underline{F}(\underline{h}^{n+1}, t_{n+1})), \quad (11)$$

which is an implicit method that is solved through the following predictor-corrector-like strategy.

Let  $\underline{h}^0$  be the vector given by the initial conditions and suppose knowing or having computed  $\underline{h}^n$  with  $n \geq 0$ . By applying the Euler's Explicit Method to (10), the corresponding solution  $\underline{h}^{n+1,1}$  at time  $t_{n+1}$  is

$$\underline{h}^{n+1,1} = \underline{h}^n + \Delta t \underline{F}(\underline{h}^n, t_n) \quad n = 0, 1, \dots, N_t - 1. \quad (12)$$

By using (11), it is possible to construct

$$\begin{aligned} \underline{h}^{n+1,r} &= \underline{h}^n + \frac{\Delta t}{2} (\underline{F}(\underline{h}^n, t_n) + \underline{F}(\underline{h}^{n+1,r-1}, t_{n+1})), \quad r = 2, 3, \dots, R, \\ \underline{h}^{n+1} &= \underline{h}^{n+1,R}, \end{aligned} \quad (13)$$

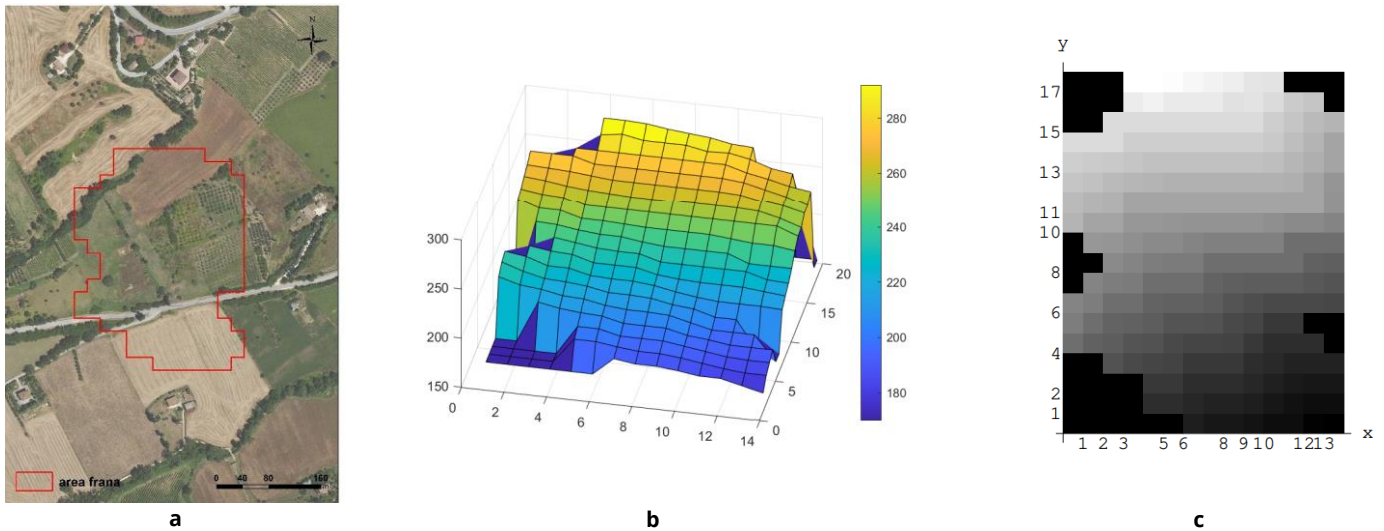
where  $R$  is the first integer that satisfies

$$\|h_{i,j,k}^{n+1,R} - h_{i,j,k}^{n+1,R-1}\|_{\infty} < tol, \quad (14)$$

and  $tol$  is an adequate tolerance.

## 5. Results and Discussion

The proposed numerical method for the construction of a hazard map has been tested on a landslide that occurred in March 2015 in the province of Ancona (Italy). This region is shown in Fig. (2a) inside the red polygonal curve, while a 3D graph of the used approximations of the corresponding altitudes is in Fig. (2b) and a 2D approximation is shown in Fig. (2c). Such approximated altitudes vary from 175m (blue in Fig. (2b), black in Fig. (2c)) to 292m (yellow in Fig. (2b), white in Fig. (2c))



The Italian region used in the simulation.

3D approximation of the corresponding altitudes.

2D approximation of the corresponding altitudes.

**Figure 2:** Italian region and approximation of its altitudes.

in Fig. (2b), white in Fig. (2c)). The bounding box  $[0, L_x] \times [0, L_y] \times [0, L_z]$  is given by  $L_x = 280m$ ,  $L_y = 360m$ ,  $L_z = 137m$ , in particular, it has been considered a soil depth of  $20m$  over the bedrock. The discretization steps are:  $\Delta x = \Delta y = 20m$ ,  $\Delta z = 1m$ , thus the bounding box has been partitioned in  $N_x = 14$ ,  $N_y = 18$ ,  $N_z = 137$  points along the  $x, y, z$  directions, respectively. It is worth noting that, with this choice, the region is contained in the bounding box, with the convention that the area with the highest altitude corresponds to a point with  $z = 137$ .

For the recharge and the evapotranspiration, data gathered by weather stations in the three months preceding the landslide event have been used. In particular, Fig. (3) shows the millimeters of rainfall in the considered period, with a measurement every 15 minutes. These data were used in the hydrological model to obtain, at each time step, the height of the water table  $z_w$  and then to compute the safety factor  $F$  in Formula (2) at each grid point corresponding to a vertical soil section between the Earth surface and the bedrock. On each vertical soil section, the depth  $z$  of the failure surface was chosen to be equal to the soil depth. Furthermore, the geomorphological information about the region was used for obtaining the various parameters present in the two models, such as, for example, the slope  $\beta$  of the inclined surface and the angle  $\phi$  of internal friction.

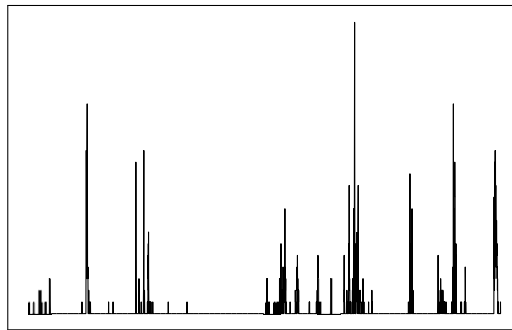


**Figure 3:** Millimeters of rain fallen every 15 minutes during the three months preceding the considered landslide event.

The results of this simulation, shown in Fig. (4), confirm that the proposed method can be effectively used to numerically construct hazard maps. Indeed, Fig. (4) shows the evolution of these hazard maps from 90 days before the landslide event to 10 days before. In particular, the legend reads that

- a black zone represents an unstable region ( $F \leq 1$ );
- a grey zone represents a stable region ( $F > 1$ );
- a white zone represents a not-considered region.

The computational time of the numerical simulations was not logged, as the aim of this study is to assess the reliability of the proposed method. However, in some preliminary simulations carried out over large areas, the results were obtained within the time needed to make forecasts. This means that, after receiving weather data for the current day, the results arrive within a few hours and allow forecasts to be made for the following day.

Finally, it is worth noting that, in Fig. (4), 60 days before the landslide, black zones started to emerge. Of course, there are no temporal hints in such information. This suggests to investigate the emerging risk areas through more accurate methods for a more reliable evaluation of the safety factor.

## 6. Conclusions

In this work, a numerical method to analyze the hazard of slope failure during rainfall events has been proposed. Regarding the equilibrium analysis, the simplest model has been considered, i.e., the infinite slope model. Nevertheless, the novelty of our approach is that the soil moisture information at the event time has been obtained by computing the numerical solution of a hydrological model [29] and from the weather station data, without resorting to statistical and historical information, as it usually happens. The proposed method has successfully built a hazard map agreeing with a real landslide.



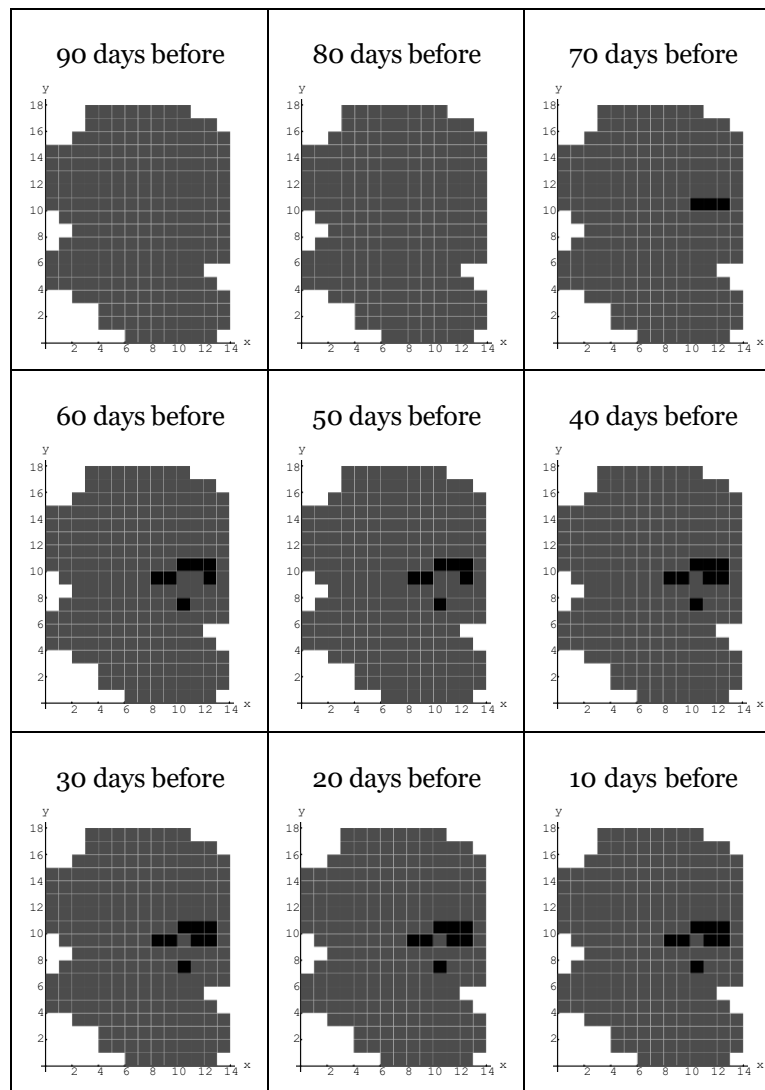


**Figure 4:** The graphical representation of the safety factor computed  $DD$  days before the considered landslide event.

In future works, the idea is to first compute the factor of safety with the *infinite slope model* for large-scale landslide hazard analysis and create a quantitative hazard map, as the one shown in this work. Then, the factor of safety should be computed with the *method of slices* for small-scale landslide hazard analysis. Such a method is more accurate but with a higher computational cost because it computes the factor of safety from a numerical solution of a suitable nonlinear system of algebraic equations. In this way, the quantitative hazard map, obtained with the infinite slope model, can be leveraged to determine limited zones, on which to perform a small-scale landslide hazard analysis through the method of slices.

In the future, some comparisons with statistical methods should be performed, as well as some additional tests on real case studies. These last tests would be particularly useful to validate the proposed method and eventually to formulate and validate a hypothesis on the minimum ratio between stable and unstable areas, in the interested region, that can trigger a landslide. Besides, several other developments need to be considered. For example, more refined numerical techniques for the algebraic system from the limit equilibrium model need to be studied, to assure a more accurate evaluation of the safety factor. Furthermore, the proposed system can be integrated with models of runoff and flood risk.

## Conflict of Interest

The authors have no conflicts of interest to disclose.

## Funding

This research received partial funding from Unione Europea – FSE, through Ministero dell'Università e della Ricerca within the call for the project Pon Ricerca e Innovazione 2014-2020 in Decreto Ministeriale 1062-10/08/2021.

## Acknowledgements

The authors would like to express their gratitude to the European Community for funding the LANDSLIDE project, as well as to the whole partnership for actively participating in this challenging research.

## References

- [1] Brown WM, Cruden DM, Denison JS. The directory of the world landslide inventory. U.S. Geological Survey; 1992, Open-File Report 92-427-A. <https://doi.org/10.3133/ofr92427A>
- [2] Lacasse S, Nadim F, Kalsnes B. Living with landslide risk. *Geotech Eng J SEAGS AGSSEA* 2010; 41: 239-67.
- [3] Crescenzo G, Pirone M, Santo A, Urciuoli G, Leroi E. SafeLand Living with landslide risk in Europe: Assessment, effects of global change, and risk management strategies. European Union; 2010.
- [4] Busslinger M. Landslide time-forecast methods. Rapperswil: HSR University of Applied Sciences; 2009.
- [5] Guzzetti F, Peruccacci S, Rossi M, Stark CP. Rainfall thresholds for the initiation of landslides in central and southern Europe. *Meteorol Atmos Phys*. 2007; 98: 239-67. <https://doi.org/10.1007/s00703-007-0262-7>
- [6] Baum RL, Godt JW. Early warning of rainfall-induced shallow landslides and debris flows in the USA. *Landslides*. 2010; 7: 259-72. <https://doi.org/10.1007/s10346-009-0177-0>
- [7] Baum RL, Savage WZ, Godt JW. TRIGRS: a Fortran program for transient rainfall infiltration and grid-based regional slope-stability analysis, version 2.0. US Geological Survey Open-File Report 2008.
- [8] Polarski M. Distributed rainfall-runoff model incorporating channel extension and gridded digital maps. *Hydrol Processes*. 1997; 11: 1-11. [https://doi.org/10.1002/\(SICI\)1099-1085\(199701\)11:1<1::AID-HYP388>3.0.CO;2-G](https://doi.org/10.1002/(SICI)1099-1085(199701)11:1<1::AID-HYP388>3.0.CO;2-G)
- [9] Schreider SY, Jakeman AJ, Pittock AB. Modeling rainfall-runoff from large catchment to basin scale: The Goulburn Valley, Victoria. *Hydrol Processes*. 1996; 10: 863-76. [https://doi.org/10.1002/\(sici\)1099-1085\(199606\)10:6<863::aid-hyp376>3.0.co;2-8](https://doi.org/10.1002/(sici)1099-1085(199606)10:6<863::aid-hyp376>3.0.co;2-8)
- [10] Giacomini J, Khamitova G, Maponi P, Vittori S, Fioretti L. Water flow and transport in porous media for in-silico espresso coffee. *Int J Multiphase Flow*. 2020; 126: 103252. <https://doi.org/10.1016/j.ijmultiphaseflow.2020.103252>
- [11] Giacomini J, Invernizzi MC, Maponi P, Verdoya M. Testing a model of flow and heat transfer for u-shaped geothermal exchangers. *Adv Model Anal A*. 2018; 55: 151-7. [https://doi.org/10.18280/ama\\_a.550308](https://doi.org/10.18280/ama_a.550308)
- [12] Richards LA. Capillary conduction of liquids through porous mediums. *Physics*. 1931; 1: 318-33. <https://doi.org/10.1063/1.1745010>
- [13] Haverkamp R, Vauclin M, Touma J, Wierenga PJ, Vachaud G. A comparison of numerical simulation models for one-dimensional infiltration. *Soil Sci Soc Am J*. 1977; 41: 285-94. <https://doi.org/10.2136/sssaj1977.03615995004100020024x>
- [14] Kirkland MR, Hills RG, Wierenga PJ. Algorithms for solving Richards' equation for variably saturated soils. *Water Resour Res*. 1992; 28: 2049-58. <https://doi.org/10.1029/92WR00802>
- [15] Onda Y. Influence of water storage capacity in the regolith zone on hydrological characteristics, slope processes, and slope form. *Zeitschrift Für Geomorphologie*. 1992; 36: 165-78. <https://doi.org/10.1127/zfg/36/1992/165>
- [16] Cheng YM, Lau CK. Slope stability and stabilization new methods and insight, second edition. London: Taylor & Francis; 2014. <https://doi.org/10.1201/b17015>
- [17] Huang C-C, Tsai C-C, Chen Y-H. Generalized method for three-dimensional slope stability analysis. *J Geotech Geoenviron Eng*. 2002; 128: 836-48. [https://doi.org/10.1061/\(ASCE\)1090-0241\(2002\)128:10\(836\)](https://doi.org/10.1061/(ASCE)1090-0241(2002)128:10(836))
- [18] Coulomb CA. Essai sur une application des règles de maximis et minimis à quelques problèmes de Statique, relatifs à l'Architecture. *Mem Div Sav Acad* 1773.
- [19] Mohr O. *Abhandlungen aus dem Gebiete der Technischen Mechanik*, 2nd ed. Berlin: W Ernst & Sohn 1914.
- [20] Yokoi H. Relationship between soil cohesion and shear strength. *Soil Sci Plant Nutr*. 1968; 14: 89-93. <https://doi.org/10.1080/00380768.1968.10432750>
- [21] Haefeli R. The stability of slopes acted upon by parallel seepage. *International Conference on Soil Mechanics and Foundation Engineering*, Rotterdam: 1948, p. 57-62.
- [22] Duncan JM, Wright SG, Brandon TL. *Soil strength and slope stability*. 2nd ed. John Wiley & Sons; 2014.
- [23] Pinder GF, Celia MA. *Subsurface hydrology*. John Wiley & Sons; 2006. <https://doi.org/10.1002/0470044209>
- [24] Hill MC, Banta ER, Harbaugh AW, Anderman ER. MODFLOW-2000, the US geological survey modular ground-water model; user guide to the observation, sensitivity, and parameter-estimation processes and three post-processing programs. U.S. Geological Survey; Denver: 2000, Open-File Report 2000-184. <https://doi.org/10.3133/ofr00184>

- [25] Beven K. Rainfall-runoff modelling: the primer. Wiley; 2012. <https://doi.org/10.1002/9781119951001>
- [26] van Genuchten MT. A closed-form equation for predicting the hydraulic conductivity of unsaturated soils. *Soil Sci Soc Am J.* 1980; 44: 892-8. <https://doi.org/10.2136/sssaj1980.03615995004400050002x>
- [27] Burdine NT. Relative permeability calculations from pore size distribution data. *J Pet Technol.* 1953; 5: 71-8. <https://doi.org/10.2118/225-G>
- [28] Mualem Y. A new model for predicting the hydraulic conductivity of unsaturated porous media. *Water Resour Res.* 1976; 12: 513-22. <https://doi.org/10.1029/WR012i003p00513>
- [29] Spadoni L, Gioia E, Egidi N, Maponi P. The moisture dynamics in saturated-unsaturated soil. In: *IMACS Series in Computational and Applied Mathematics.* Rome: Rosa Maria Spitaleri, Daniela Mansutti; 2017, vol. 20: pp. 161-70.
- [30] Freeze RA. Three-dimensional, transient, saturated-unsaturated flow in a groundwater basin. *Water Resour Res.* 1971; 7: 347-66. <https://doi.org/10.1029/WR007i002p00347>
- [31] Hanks RJ, Bowers SA. Numerical solution of the moisture flow equation for infiltration into layered soils. *Soil Sci Soc Am J.* 1962; 26: 530-4. <https://doi.org/10.2136/sssaj1962.03615995002600060007x>
- [32] Harbaugh A. MODFLOW-2005, the US Geological Survey modular ground-water model: the ground-water flow process. VA: 2005. <https://doi.org/10.3133/tm6A16>
- [33] Diersch H-JG. FEFLOW: finite element modeling of flow, mass and heat transport in porous and fractured media. Berlin, Heidelberg: Springer Science & Business Media; 2013. <https://doi.org/10.1007/978-3-642-38739-5>
- [34] Forsyth PA, Wu YS, Pruess K. Robust numerical methods for saturated-unsaturated flow with dry initial conditions in heterogeneous media. *Adv Water Resour.* 1995; 18: 25-38. [https://doi.org/10.1016/0309-1708\(95\)00020-J](https://doi.org/10.1016/0309-1708(95)00020-J)
- [35] Li CW. A simplified Newton Iteration Method with linear finite elements for transient unsaturated flow. *Water Resour Res.* 1993; 29: 965-71. <https://doi.org/10.1029/92WR02891>
- [36] Abriola LM, Lang JR. Self-adaptive hierarchic finite element solution of the one-dimensional unsaturated flow equation. *Int J Numer Methods Fluids.* 1990; 10: 227-46. <https://doi.org/10.1002/flid.1650100302>
- [37] Egidi N, Gioia E, Maponi P, Spadoni L. A numerical solution of Richards equation: a simple method adaptable in parallel computing. *Int J Comput Math.* 2020; 97: 2-17. <https://doi.org/10.1080/00207160.2018.1444160>